Sensors and Materials, Vol. 12, No. 4 (2000) 175–203
MYU Tokyo

S & M 0406

Resonant Microbeam Electronic Oscillators for Strain Sensing

Yongchul Ahn and Henry Guckel

Wisconsin Center for Applied Microelectronics
Department of Electrical and Computer Engineering
University of Wisconsin - Madison
1410 Engineer Dr., Madison, WI 53706, U.S.A.

(Received January 14, 2000; accepted June 13, 2000)

Key words: oscillator, microbeam, resonator, sensor, strain

Resonant clamped-clamped microbeams which are placed into a hard vacuum cavity are of interest for sensor applications. The devices are fabricated from polysilicon on a single crystal silicon substrate. They have fundamental resonant frequencies of several hundred kilohertz with quality factors as large as 300,000. The resonant frequency changes in a predictable way with applied axial load forming a highly desirable, very sensitive transduction mechanism which can be used in a variety of sensors. Accurate frequency detection requires the sinusoidal oscillation of these devices during measurements. This transduction method can provide higher resolution than voltage or current measurements typical of piezoresistive sensors. Oscillator design involves an amplifier with larger than unity gain, a phase shift of 360 degrees, and an automatic gain control circuit. To design such a circuit with the resonator as the tuning element it is useful to use computer simulation programs. This requires that the mechanical parameters for the resonator be converted to electrical equivalents. Fully functional sinusoidal oscillators with microbeams have been constructed and tested successfully. An integrated sinusoidal oscillator with an active automatic gain control (AGC) loop has produced acceptable results.

1. Introduction

Fully integrated polysilicon resonators using capacitive, magnetic, and optical sensing schemes have been developed at the Wisconsin Center for Applied Microelectronics (WCAM).[1–11] These resonators consist of clamped-clamped micromechanical polysilicon beams sealed in a vacuum cavity along with electronic sensing components. The vacuum in the cavity is chemically induced and provides a hard vacuum environment. The hard vacuum in the cavity prevents gas damping of the moving beam. The result is a high quality factor, Q, resonator. The Q of the microbeam resonator can be obtained from the measurement of the resonant frequency.[2,8] A high Q device exhibits a sharp amplitude peak near the resonant frequency. This results in high signal-to-noise ratios. The high Q devices also require a very small input power to maintain the beam vibrations and, therefore, are characterized by low power dissipation. The polysilicon beams are designed to be operated at high resonant frequency so that environmental vibrations at lower frequencies cannot excite the polysilicon beam. Typical polysilicon beams used in resonators are 200 μm in length, 40 μm in width, and 2 μm in thickness. The beam-to-substrate spacing is typically 0.8 μm. This geometry produces an unloaded fundamental resonance near 500 kHz when the polysilicon is annealed to zero built-in strain. If the polysilicon beam is excited by a sinusoidal force applied normal to its center, the beam deflection will have a maximum at this fundamental frequency. Measured Q values of the resonators can be as large as 300,000. The output of the resonators is measured in the form of resonant frequency changes. Since the resonant frequency is a function of axially applied or built-in strains in the beam, [3–5,7,8] a fractional frequency change of the resonator due to applied axial loads and strains occurs. For example, an axial load of 1 dyne, roughly 1 milligram of weight, raises the resonant frequency by approximately 250 Hz.[3,8] The input power to maintain the resonance of these devices is as low as 10^{-14} W.[1–3,8] The long term frequency stability has been measured. The drift is less than 1 ppm per month.[3,8]

Polysilicon resonators can be incorporated into sensors which measure quantities such as pressure, temperature, force and acceleration. In these devices, resonators can be used in place of piezoresistors. This is attractive because:

- Resonators show quasi-digital characteristics with good measurement stability (frequency not amplitude measurements).[1,3,4,8,10,11] Since frequency measurements produce an accurate output over 9 decades whereas voltages and currents can only be measured to six decades, this represents improved resolution.
- These devices exhibit excellent noise rejection during measurements since they are very high Q devices.
- High Q resonators have very low power dissipation which can be as small as10^{-14} W.[1–3,8]
- The devices are several orders of magnitude more sensitive to an applied load than piezoresistors. The sensitivity to applied axial loads exceeds the gage factor of piezoresistors by a factor of 10 to 100.[3,7,8]

Functional performance measurements of the resonators, such as resonant frequency, sensitivity, linearity and stability, have been carried out either at the wafer level or by packaging these devices. The output signal of the resonators is the resonant frequency, which implies time-based measurements. These measurements can be more accurately implemented than voltage or current measurements. Available equipment[12–14] substantiates this. High-performance frequency measurement systems, such as an HP5370B[13] electronic frequency counter, have more than 11 digits of resolution. High-resolution voltage and current measurement equipment provides up to 7 1/2 digits of resolution for an updated display every two seconds and 0.6 ppm accuracy for DC voltages over a 24 h period. Frequency measurements can therefore provide 3–4 more digits of measurement resolution than voltage or current measurements.

To use the resonators for an accurate frequency measurement as part of a sensor, the resonators must oscillate during the measurement. This can be implemented by making the resonator part of an oscillator circuit. Oscillators are closed loop amplifiers. Oscillator circuits generate steady state sinusoidal resonant frequencies using the resonator as a tuning element and by satisfying two conditions: the net phase around the entire loop must be zero or 360° (positive feedback) and the net gain of the loop must be one. The oscillator frequency can be measured at the output of the circuit. This method of using the resonators has several advantages:

- This method can produce micromechanical sensors which use frequency measurements to determine the value of the sensed quantity.
- The technique produces no increased power dissipation within the resonator. The power dissipation occurs in the peripheral electronic circuits rather than in the resonating device.
- The oscillator method raises the possibility of the cofabrication of a sensor and an oscillator on a single chip.

The measurement of the resonant frequency and Q via an oscillator with piezoresistors has been performed at the Wisconsin Center for Applied Microelectronics.[8] In this technique, the clamped-clamped beam is furnished with a piezoresistor to measure beam motion. Frequency sensing for this method is not very desirable since the power dissipation in the piezoresistors is large. Typical power dissipation for piezoresistors is usually in the milliwatt range.[1,9] A simple oscillator which does not increase the power consumption within the resonator is more desirable. An optically self-excited resonator[11] has been tested and found to be an excellent alternative to optothermal excitations because of reduced input optical power. However, optics cannot always be used because optics need a clean environment and the accurate alignment of optical components such as optical fibers and detectors.

An oscillator combining microelectronics with micromachined polysilicon beam resonators which involve capacitive driving and sensing schemes can produce an excellent oscillating system with very small power dissipation within the resonator. In this case, the resonator becomes a tuning element in an amplifier circuit with an automatic gain controller. The amplifier circuit must have a flat frequency response over the span of the

measuring frequency range since the oscillation frequency of the oscillator changes. The automatic gain controller keeps the oscillator in the sinusoidal operating mode.

2. Beam Controlled Oscillator Design

2.1 *Theory*

Figure 1 shows a generalized feedback system with the transfer function

$$\frac{V_o(j\omega)}{V_i(j\omega)} = \frac{H_1(j\omega)}{1 - AH_1(j\omega)} = \frac{H_1(j\omega)}{1 - A_L(j\omega)}, \tag{1}$$

where $A_L(j\omega) = AH_1(j\omega)$ is defined as the "loop gain" of the oscillator and A is the feedback factor of the system. It is apparent that the poles of the feedback oscillator are the zeros or roots of the denominator,

$$1 - A_L(j\omega) = 0 \cdot \tag{2}$$

If eq. (2) has a pair of complex conjugate roots in the right half of the s-plane, $v_o(t)$ will be a growing sinusoid even with $v_i(t) = 0$. From eq. (2) the oscillation conditions of the feedback amplifier are given by

$$\begin{aligned} &\mathrm{Re}[A_L(j\omega)] \geq 1 \\ &\mathrm{Im}[A_L(j\omega)] = 0 \end{aligned} \tag{3}$$

In eq. (1), $\mathrm{Re}[A_L(j\omega)] = 1$ gives the minimum value of the gain for the amplifier and $\mathrm{Im}[A_L(j\omega)] = 0$ gives the oscillation frequency of the system.

Two-port micromechanical beams having two capacitors for excitation and detection

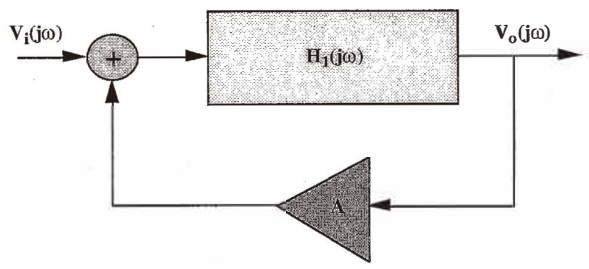

Fig. 1. Generalized feedback amplifier.

can be represented by an equivalent circuit which consists of the motion impedance, Z_m and the vacuum capacitances, C_{so} and C_{do}.[15] The system configuration is shown in Fig. 2. The value of Z_m is given by

$$Z_m = R_{eq} + j\omega L_{eq} + \frac{1}{j\omega C_{eq}} = \frac{c}{\Gamma_s^2} + j\omega\frac{m}{\Gamma_s^2} + \frac{k}{j\omega\Gamma_s^2}, \tag{4}$$

where m, c, and k represent mass, damping, and spring constant, respectively. The electromechanical coupling constants, Γ_s and Γ_d are given by

$$\Gamma_s = \frac{\varepsilon_o S_l V_{so}}{g_l^2} = \frac{C_{so} V_{so}}{g_l}, \tag{5}$$

$$\Gamma_d = \frac{\varepsilon_o S_u V_{do}}{g_u^2} = \frac{C_{do} V_{do}}{g_u}, \tag{6}$$

where ε_o denotes vacuum permittivity, g_l is the gap between the beam and the lower plate, g_u is the gap between the beam and the upper plate, S_l is the area of the lower capacitor plates, S_u is the area of the upper capacitor plates, V_{so} and V_{do} are the applied DC voltages, $C_{so} = \varepsilon_o S_l / g_l$, and $C_{do} = \varepsilon_o S_u / g_u$.

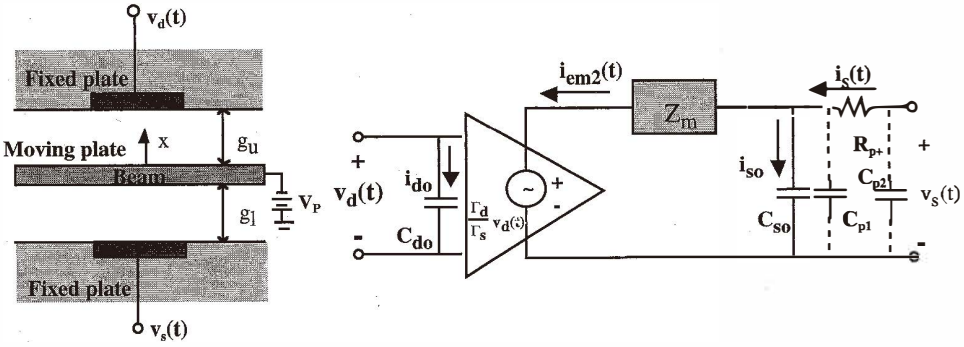

Fig. 2. Schematics of the electrostatically driven and sensed two-port beam resonator and its electrical equivalent circuit. (a) Two-port beam resonator system; and (b) electrical equivalent circuit.

A basic oscillator using a NMOS amplifier and a micromechanical resonator is shown in Fig. 3(a). The oscillation requirements of the feedback circuit can be found from the calculation of the open-loop gain for the circuit. In this method, the feedback loop has been broken at the input to the forward gain path, and a dummy input $v_i(t)$ has been inserted to allow examination of the loop transfer characteristic. In Fig. 3(a), the circuit is broken at node *a* and connected to an input $v_i(t)$. The general form of the open-loop circuit is shown in Fig. 3(b). The open-loop gain is calculated as

$$H_1(j\omega) = \frac{V_o(j\omega)}{V_i(j\omega)} = \frac{(\Gamma_d / \Gamma_s)(Z_1Z_2 - g_m Z_1 Z_2 Z_3)}{Z_m(Z_1 + Z_2 + Z_3) + Z_1Z_2 + Z_1Z_3}. \quad (7)$$

The oscillator is the result of shorting the input and output of the open-loop circuit. Since the input node *a* is connected with the output for a closed-loop circuit, the feedback factor, A of the circuit in eq. (1), is one. Therefore, the loop gain, $A_L(j\omega)$, is the same as the open-loop gain in eq. (7). Oscillations may occur only if the small-signal open-loop gain of the circuit is greater than unity and its phase is equal to zero at the frequency of resonance. The open-loop gain-phase measurement can be applied directly to the construction of the oscillator.

2.2 *Design considerations for microbeams*

The basic electrical connections for an electrostatic drive and sense microbeam resonator are shown in Fig. 2(a). The fundamental difference between electrostactically driven beam resonators and quartz crystal resonators lies in the nonlinearity of the equations governing the electrostatic excitations. The extracted electrical components, such as inductance, resistance and capacitance, of the equivalent circuit of the beam resonator depend on the DC polarization voltage applied to the beam.[15] This results in the possibility of mechanical instability and a lowering of *Q*. This also results in driving

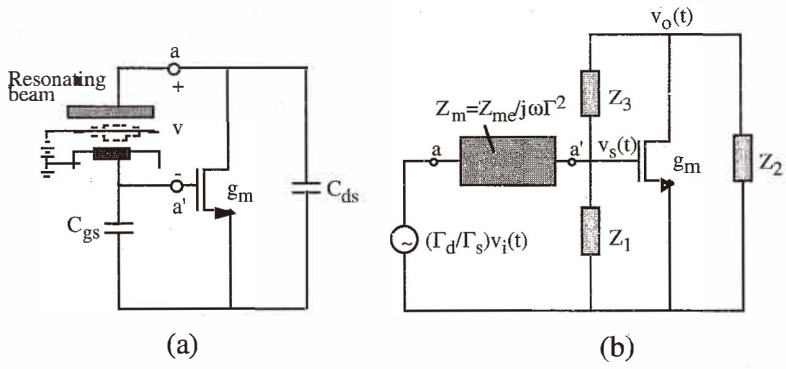

Fig. 3. Configuration of an oscillator using a NMOS amplifier and a two-port microbeam resonator: (a) closed loop circuit, and (b) open loop circuit where $Z_{me} = k + j\omega c - \omega^2 m$.

voltage requirements for linear microbeam operation. Parasitics of the electrostatically driven microbeam can also be a problem for oscillator performance.

2.2.1 *Driving voltage requirements for linear operations*

The driving voltage requirements for simple beams, which have the beam dimensions of length L, width W, thickness h, material density ρ, and Young's modulus E, for linear operation have been obtained[15] and are described by

$$V_{DC}v_{ac} < \frac{1.4}{Q^{1.5}} \frac{\rho LWh^2 g^2}{\varepsilon_o S} \frac{\omega_o^3}{\omega_n}, \tag{8}$$

where

$$\omega_o = \omega_n \sqrt{1 + \frac{2\varepsilon L^2}{7h^2}}, \tag{9}$$

and

$$\omega_n = \sqrt{\frac{42Eh^2}{\rho L^4}}. \tag{10}$$

ε is the total axial strain of the microbeam, ε_o is vacuum permittivity, and S is the area of the driving capacitor. Equation (8) suggests that a high Q microbeam needs to have small driving voltages for linear operation. This means that it is very difficult to implement the beam controlled oscillator with very high Q devices. Therefore, Q variations must be considered for the driving voltage conditions of the microbeam resonators in the oscillator design.

2.2.2 *Electric field effects on resonant frequency and quality factor*

The value of Q for a resonating beam is determined not only by residual gas in the cavity but also by the support losses and by the electrical losses induced by the vibrating polysilicon capacitor composed of the microbeam and the bias electrode. Q values depend on the method of fabrication and measurement. The resonant frequency depends on the dimensions, geometry and material properties of the resonant beam. The resonant frequency and Q can also depend significantly on the DC bias and AC drive level used for excitation.

The Q changes can be understood in terms of a parasitic electrical resistance connected in series with the motional impedance in the driven circuit. The analysis is based on the equation of motion of the microbeam driven by the circuit shown in Fig. 4.[15,16]

The DC bias effects on the resonant frequency and Q of the two-port microbeam

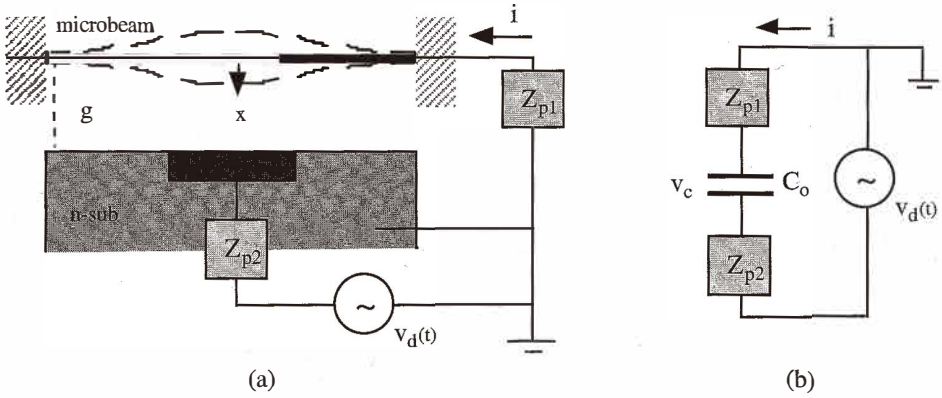

Fig. 4. Schematic diagram for the analysis of Q and resonant frequency changes by the driving electric field.

resonators have been investigated in the references.[15,16] From Fig. 4, the linearized equation of motion in terms of x and v_c can be obtained and is given by

$$m\frac{d^2x}{dt^2}+c\frac{dx}{dt}+k(1-\kappa^2)x=\frac{C_oV_{DC}}{g}v_c=\Gamma v_c, \tag{11}$$

where Γ is the electromechanical conversion parameter and $\kappa^2=C_oV_{DC}^2/kg^2$. This equation shows that the spring constant is reduced fractionally by an amount κ^2 proportional to V_{DC}^2. The resonant frequency and the quality factor with an applied electric field can be obtained from eq. (11) and are described by

$$\omega_R^2=\frac{k}{m}(1-\kappa^2\frac{1-C_o/C_p}{1+\omega_R^2\tau^2})=\omega_o^2(1-\kappa^2\frac{1-C_o/C_p}{1+\omega_R^2\tau^2}), \tag{12}$$

and

$$\frac{1}{Q}=\frac{c}{m\omega_R}+\frac{\Gamma^2}{m\omega_R}\frac{R_p}{1+\omega_R^2\tau^2}=\frac{1}{Q_o}\frac{\omega_o}{\omega_R}+\frac{\Gamma^2}{m\omega_R}\frac{R_p}{1+\omega_R^2\tau^2}, \tag{13}$$

where Q_o and ω_o are the unperturbed quality factor and resonant frequency, respectively, and $\tau^2=C_o^2Z_pZ_p^*$. The parasitic impedance Z_p contains the parasitic resistance R_p and the

parasitic capacitance, C_p. Equations (12) and (13) indicate that the resonant frequency and the quality factor of the electrostatically driven microbeam are influenced significantly by the DC bias. Therefore, in the oscillator design, the DC bias is an important parameter since it influences characteristics of the performance of the resonator circuit such as oscillation frequency drifts and power dissipation.

2.2.3 *Parasitic effects on beam resonator performance*

Parasitic electrical components of the mechanical microbeam resonator such as interconnection resistance and capacitance are of great importance in designing an oscillator using the combination of an MOS amplifier and a resonating beam. These parasitics affect the oscillation behavior of the system, particularly the gain and phase response of the resonator.

The difference between one-port and two-port beam resonators lies in the use of driving and sensing electronic structures. The one-port devices have one parallel-plate capacitor, so the driving and sensing operations are performed by the same electrode pair. Since the driving and sensing signals in these devices are coupled during operation, a fairly large capacitor is required to increase the sensitivity. The two-port beam resonators have a separate driving and sensing electronic structures. The coupling factor of the driving and sensing signals is presumed to be low. Figure 5 shows cross-sectional views of one-port and two-port beam resonators.

The parasitic effects on the beam resonator performance for one-port and two-port systems have been qualitatively discussed in ref. (15). Figure 6 shows the measured gain-phase spectra of one-port and two-port devices. As evident in Fig. 6, the deterioration of the gain-phase of the one-port device by parasitics is more severe than that of the two-port device. This results from the parasitic capacitance between driving and sensing electrodes of the one-port devices which is larger than that of the two-port devices.[15] It is concluded that resonators configured as a two-port system give the best results in terms of a high signal-to-noise ratio and a small influence of parasitic loads. Therefore, the two-

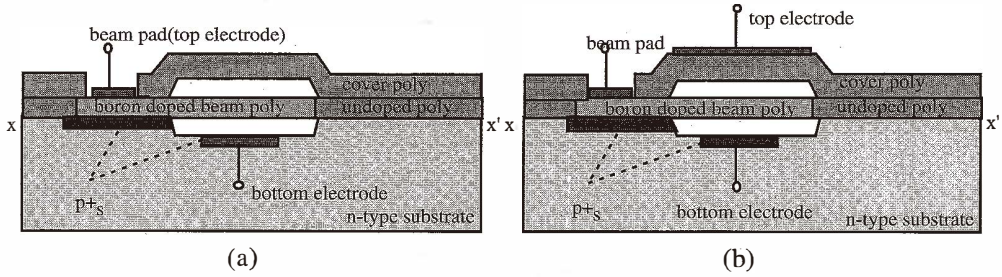

Fig. 5. Cross-sectional views of one-port and two-port beam resonators. (a) One-port beam resonator and (b) two-port beam resonator.

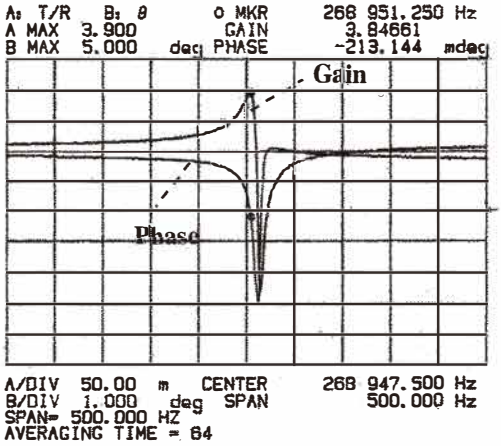

(a)

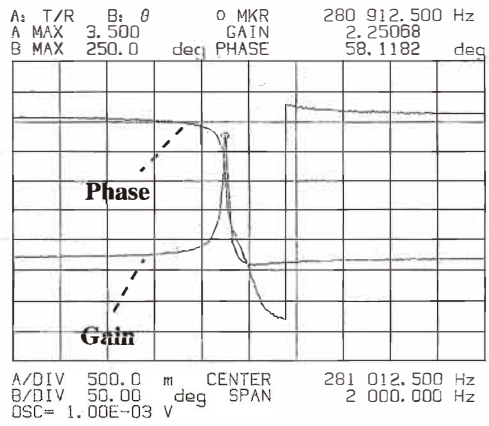

(b)

Fig. 6. Open loop gain-phase spectra of (a) one-port and (b) two-port beam resonators. (a) One-port: the resonant frequency is about 269 kHz. The signal-to-noise ratio at resonance is about 1.04. The phase change going through resonance is barely 5°. (b) Two-port: The resonant frequency is about 280.7 kHz. The signal-to-noise ratio at resonance is about 9.0. The phase change going through resonance is a full 180°.

port device has advantages over the one-port device for an electronic beam controlled oscillator.

2.3 *Oscillator using a microbeam and a MOS amplifier*

A design for an oscillator circuit using a microbeam and a three-stage NMOS amplifier has been developed using electromechanical transduction parameters of the microbeam inductance, resistance and capacitance. Figure 7 shows the schematic diagram of this oscillator circuit. The beam controls the oscillation frequency. The three-stage NMOS amplifier amplifies the resonant signal to make the entire net gain greater than one. C_1 and C_2 of the circuit decouple the DC biasing of the NMOS amplifier and the beam resonator.

To compute the open-loop gain, the circuit is broken at node *a* in Fig. 7. The small-signal equivalent circuit can be modeled as shown in Fig. 8. Parasitic electrical effects of the NMOS transistors such as C_{gs}, C_{gd}, C_{ds}, and r_{ds} are included in the loop gain calculation along with the parasitics in the beam resonator. The description of the impedances is as follows.

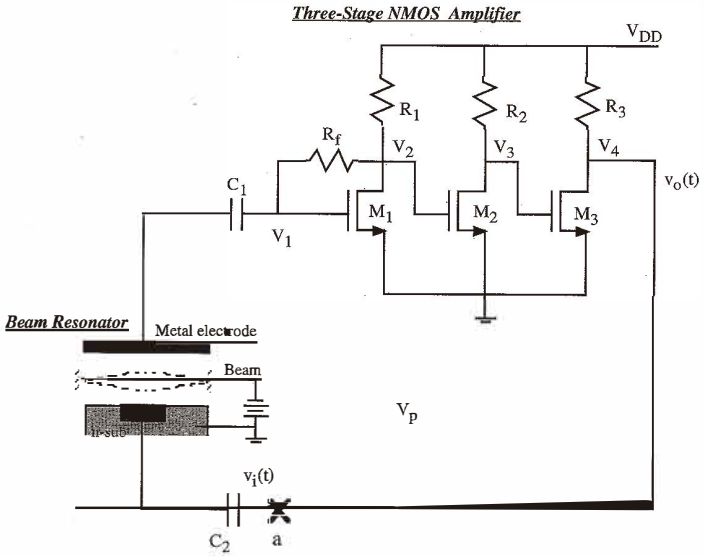

Fig. 7. Schematic diagram of a sinusoidal oscillator circuit controlled by the beam resonant frequency. The oscillator consists of a microbeam resonator and a three-stage NMOS amplifier.

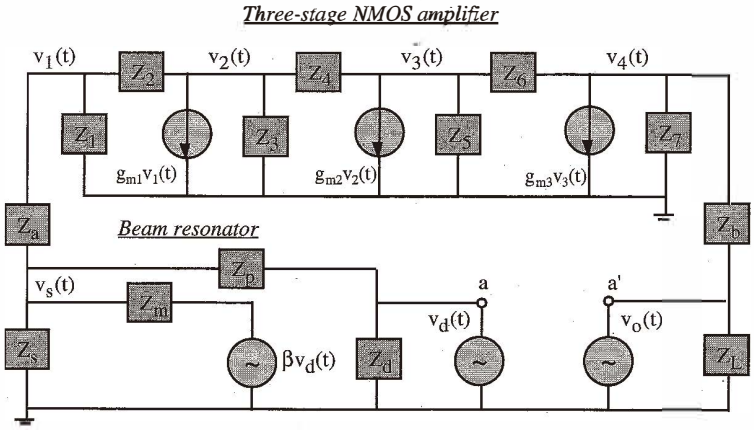

Fig. 8. Small-signal equivalent circuit for open-loop gain calculation.

$$\begin{cases} Z_d = R_{p1}/[1+j\omega R_{p1}(C_{do}+C_{p1})] & Z_1 = 1/j\omega C_{gs\ 1} \\ Z_p = 1/j\omega C_{p3} & Z_2 = R_f/(1+j\omega R_f C_{gd1}) \\ Z_m = R_{eq} + j\omega L_{eq} + 1/j\omega C_{eq} & Z_3 = r_{ds1}/[1+j\omega r_{ds1}(C_{dsl}+C_{gs1})] \\ Z_s = R_{p2}/[1+j\omega R_{p2}(C_{so}+C_{p2})] & Z_4 = 1/j\omega C_{gd2} \\ Z_a = 1/j\omega C_1 & Z_5 = r_{ds2}/[1+j\omega r_{ds2}(C_{ds2}+C_{gs3})] \\ Z_b = 1/j\omega C_2 & Z_6 = 1/j\omega C_{gd3} \\ Z_L = R_L/(1+j\omega R_L C_L) & Z_7 = r_{ds3}/(1+j\omega r_{ds2} C_{ds2}) \end{cases} \tag{14}$$

The parameter β in Fig. 8 is the ratio of the electromechanical conversion parameters for the driving and sensing capacitors and is given by

$$\beta = \Gamma_d / \Gamma_s , \tag{15}$$

where Γ_d and Γ_s are electromechanical coupling constants for the driving and sensing structures, respectively. For the circuit in Fig. 8, the open-loop gain is calculated as

$$H(j\omega) = \frac{V_o(j\omega)}{V_d(j\omega)} = \prod_{i=1}^{6} A_i = A_1 A_2 A_3 A_4 A_5 A_6 , \tag{16}$$

where

$$A_1 = \frac{V_o(j\omega)}{V_4(j\omega)} = \frac{Z_L}{Z_L + Z_b} , \tag{17}$$

$$A_2 = \frac{V_4(j\omega)}{V_3(j\omega)} = \frac{Z_6^{-1} - g_{m3}}{Z_6^{-1} + Z_7^{-1} + Z_b^{-1} - G_1 Z_b^{-1}} , \tag{18}$$

$$A_3 = \frac{V_3(j\omega)}{V_2(j\omega)} = \frac{Z_4^{-1} - g_{m2}}{Z_4^{-1} + Z_5^{-1} + Z_6^{-1} - G_2 Z_6^{-1}} , \tag{19}$$

$$A_4 = \frac{V_2(j\omega)}{V_1(j\omega)} = \frac{Z_2^{-1} - g_{m1}}{Z_2^{-1} + Z_3^{-1} + Z_4^{-1} - G_3 Z_4^{-1}} , \tag{20}$$

$$A_5 = \frac{V_1(j\omega)}{V_s(j\omega)} = \frac{Z_a^{-1}}{Z_1^{-1} + Z_2^{-1} + Z_a^{-1} - G_4 Z_2^{-1}}, \tag{21}$$

$$A_6 = \frac{V_s(j\omega)}{V_d(j\omega)} = \frac{Z_p^{-1} + \beta Z_m^{-1}}{Z_p^{-1} + Z_m^{-1} + Z_s^{-1} + Z_a^{-1} - G_5 Z_a^{-1}}. \tag{22}$$

If eq. (16) meets the condition that the gain is greater than unity and its phase is equal to zero, oscillations will occur.

The calculation of the open-loop gain and phase using eq. (16) is tedious, but plotting the gain-phase diagram of the open-loop gain as a function of frequency offers a simple method of determining the electrical components for an oscillator. The oscillation condition can also be determined by measuring the open-loop gain-phase response of the circuit. An example is shown in Fig. 9. Figure 9 shows the open-loop gain and phase diagram of a circuit, which consists of a beam resonator and a three-stage NMOS amplifier. Electrical parameters of the NMOS transistors such as transconductance and parasitic capacitances are selected to meet the oscillation conditions using the open-loop analysis. The parameters for the calculation are given in Table 1. As shown in this table, the calculation indicates that the frequency at zero phase is about 279.9 kHz. The open-loop gain at this frequency is greater than unity. Therefore, oscillations will occur when this circuit is converted to a closed-loop circuit by connecting nodes *a* and *a'* of Fig. 8. The oscillation frequency is the frequency at zero phase, which is about 279.9 kHz for this example. This graphical analysis is mainly used for experimentally determining the oscillation conditions.

2.4 *Simulation program with integrated circuit emphasis (SPICE) simulations*

Circuit simulations are performed on the oscillator, which consists of a resonant microbeam and a three-stage NMOS amplifier, using HSPICE.[17] The schematic diagram of the circuit simulated by the SPICE program is the same as in Fig. 7. The mechanical structure of the microbeam is first converted to equivalent passive electric components. These components are then combined with a three-stage NMOS amplifier and other components to form the total oscillator circuit for the SPICE simulator. The component values of the oscillator circuit are described in Table 1. The SPICE simulation results are shown in Fig. 10. Figure 10 shows the transient response of the oscillator and its waveform over a small period of time. As shown in Fig. 14, the oscillation starts to build up 1.3 ms after the power supply is turned on. The oscillation frequency of the simulated circuit is about 280 kHz, which is the same as the resonant frequency of the microbeam.

3. Experimental Results and Discussions

3.1 *Experimental*

The microstructures of the resonant devices are fabricated by depositing layers of polysilicon and sacrificial silicon dioxide and nitride to fabricate a microbeam clamped at

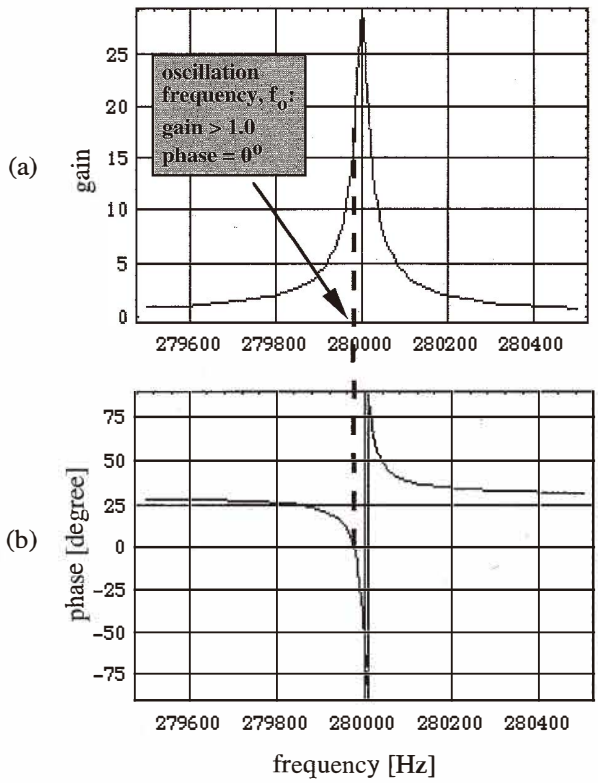

Fig. 9. Gain-phase response of an open-loop circuit. The frequency at phase = 0° is about 279.9 kHz, which is the oscillation frequency for a closed-loop circuit. The gain is greater than unity at that frequency. (a) Gain response and (b) phase response as a function of frequency.

both ends and encased in the integrated hard vacuum cell. The two-port beam resonators which contain separate electronic structures for excitation and detection are selected for the implementation of the beam controlled oscillator. The details of the fabrication process are described in ref. (15). Figure 11 shows a SEM photograph of a fabricated microbeam resonator.

Figure 12 shows the diagram for the open-loop and closed-loop measurements for the beam controlled oscillator circuit. The circuit consists of the three-stage NMOS amplifier and the beam resonator. The beam in the resonator is negatively DC-biased to ground. As mentioned before, the capacitances C_1 and C_2 decouple the DC-biasing conditions between the three-stage NMOS amplifier and the beam resonator. The three-stage NMOS amplifier and the packaged beam resonator were built on a test board and placed in a

Table 1
Parameters to calculate the gain-phase for the open-loop circuit.

Mechanical parameters		
Beam dimension	length/width/thickness	400 μm/56 μm/2.1 μm
Driving plate area, S_d		120×56 μm^2
Sensing plate area, S_d		400×56 μm^2
Space between beam and lower plate, g_l		0.85 μm
Space between beam and upper plate, g_u		0.85 μm
Assumed data	Resonant frequency, f_R	280 kHz
	Quality factor, Q	10000
V_p		-1.0 V
Parasitics C_{p1}, C_{p2}		1 pF
C_{p3}		0.5 fF
R_{p1}		100 MΩ
R_{p2}		100 GΩ
NMOS parameters		
Transconductance, g_{m1}, g_{m2}, g_{m3}		0.15 mS
C_{gs1}, C_{gs2}, C_{gs3}		2 pF
C_{ds1}, C_{ds2}, C_{ds3}		1 pF
C_{gd1}, C_{gd2}, C_{gd3}		1 pF
r_{ds1}, r_{ds2}, r_{ds3}		10 MΩ
Other electrical components		
R_1, R_2, R_3		15 kΩ
R_f		5 MΩ
C_1, C_2		10 nF

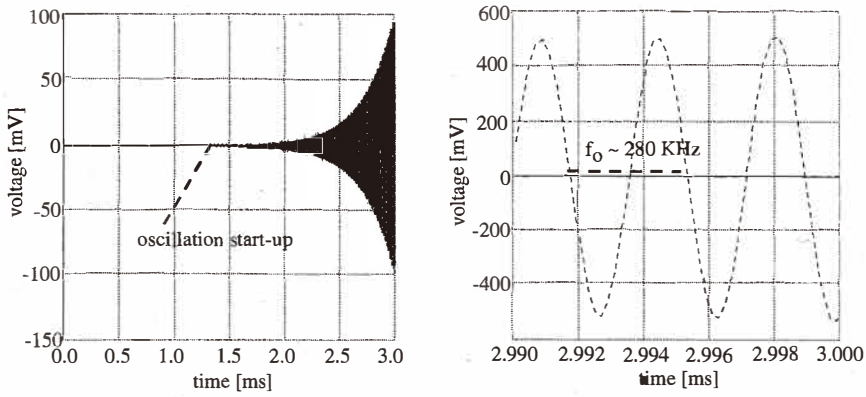

Fig. 10. SPICE simulation results. The oscillation starts to build up 1.3 ms after the power supply is turned on. The oscillation frequency is about 280 kHz, which is the same as the resonant frequency of the microbeam: (a) Transient response of the oscillator and (b) its waveform as a function of time.

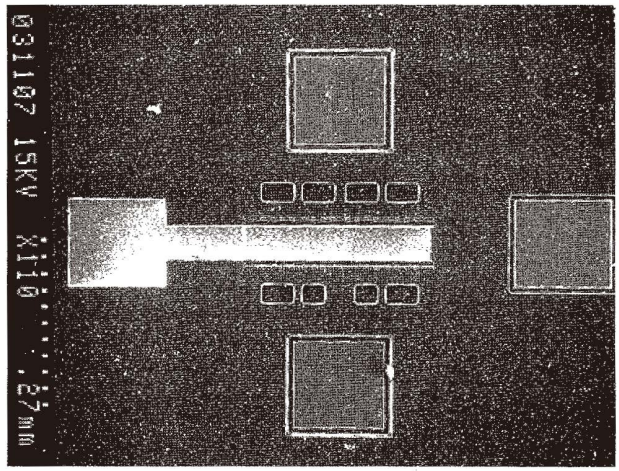

Fig. 11. SEM photograph of a fabricated two-port beam resonator. The beam has the dimensions of length $L = 300$ μm, width $W = 56$ μm, and thickness $h = 56$ μm.

shielded aluminum box. The operation of the open-loop measurement in Fig. 12 is as follows:

(1) Node a is connected to the output channel of an HP4194A gain-phase analyzer which produces the input AC signal, $v_i(t)$ as a function of frequency.
(2) The AC signal, $v_i(t)$, along with the DC voltage V_p generates an electrostatic force on the beam causing the beam to vibrate.
(3) The beam vibration is capacitively sensed by the upper capacitor.
(4) The sensed signal is amplified by the three-stage NMOS amplifier.
(5) The amplified signal $v_o(t)$ at the node a' is connected to the test channel of the HP4194A gain-phase analyzer and is compared with the input signal.

For the closed-loop measurement, node a and a' are connected together as shown in Fig. 12. The oscillation waveform and frequency were monitored by connecting node a (a') to the oscilloscope channel. In this measurement, two oscilloscopes, the Tektronix TDS 420A digitizing oscilloscope and the Tektronix 2236 oscilloscope, were used. The input impedance of the Tektronix TDS 420A digitizing oscilloscope is 1 MΩ//15 pF and that of the Tektronix 2236 oscilloscope is 1 MΩ// 22 pF. The input impedance for the HP4194A gain-phase analyzer is 1 MΩ//28 pF. The differences in the input impedances may cause a slight change in phase of the oscillator and, therefore, there is a small difference in the oscillation frequency of the oscillator circuit measured by the various systems. This

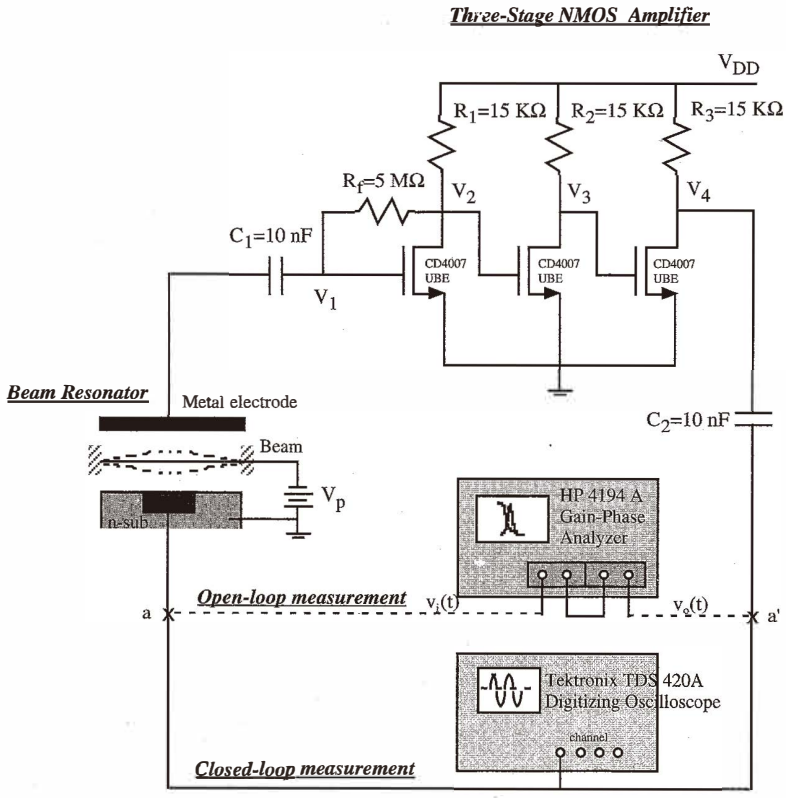

Fig. 12. Diagram for the open-loop and closed-loop gain measurements.

means that these input impedances must be considered in analyzing the loop gain and phase of the oscillator circuit.

3.2 *Closed-loop measurements for beam controlled oscillator*

The closed-loop measurement results for the beam controlled oscillator are presented in this section. The closed-loop measurements use the results of the open-loop measurements to find if the gain and the phase satisfy the oscillation conditions.

Figure 13 shows the gain-phase spectrum of a 400 μm simple beam using the open loop measurement. The plot in Fig. 13 (a) states that the frequency at 0° is about 280.915 kHz and the gain at this frequency is about 1.5, which satisfies the oscillation conditions. The measured Q is 16,037. Measurements for other unwanted signals generated from the circuit components which may dominate this resonant signal were also performed. If the other signals meet the oscillation conditions and their gains are greater than the gain from the beam resonator, the oscillation of the circuit may occur at the frequencies produced by

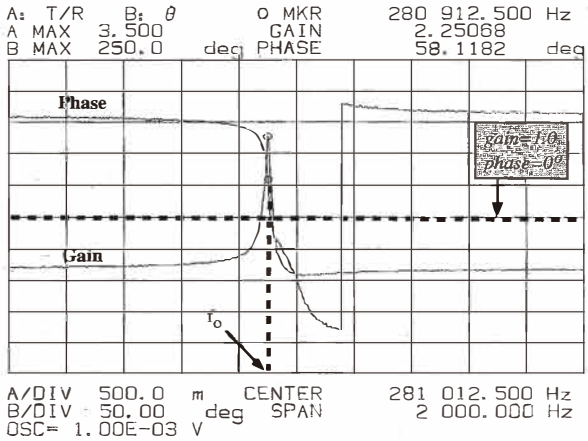

(a)

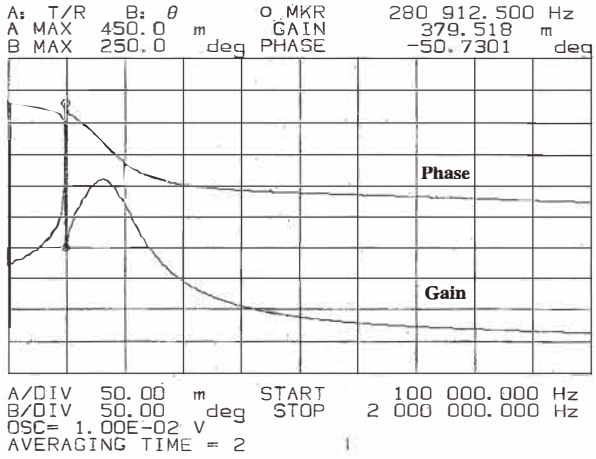

(b)

Fig. 13. Open-loop measurement of a 400 μm simple beam with V_{DD} = 5.0 V and V_p = – 0.25 V. (a) The frequency f_o at 0° phase is about 280.915 kHz. The gain at this frequency is about 1.5. (b) There are no other signals except the resonant signal at the frequency of about 281 kHz between 100 kHz and 2 MHz.

the circuit components and not the frequency produced by the beam resonator. Measurement results are shown in Fig. 13(b). This figure contains the gain-phase spectrum for a frequency range from 100 kHz to 2 MHz. In Fig. 13(b), no other signals except the signal produced by the beam resonator are observed. Therefore, the circuit with the combination of the beam resonator and the three-stage NMOS amplifier is ready for self-excited oscillations controlled by the beam resonance in closed-loop operation. The same procedure to find the oscillation condition was also performed on a 300 μm simple beam. The experimental results were that the oscillation frequency at 0° is measured as 402.766 kHz and the gain at this frequency is about 1.1. The measured Q is 19,178. No other signals in the gain-phase spectrum with a frequency range of 100 kHz to 2 MHz could be found except the resonant signal of the beam.

To obtain the oscillation behavior in the closed circuit, nodes a and a' in Fig. 12 were connected together. Figure 14(a) shows the evolution of the oscillations for a 400 μm simple beam resonator after turn-on. From the oscillogram in Fig. 14 (a), the starting time of the oscillation for a 400 μm beam resonator is about 200 ms after the DC-bias is turned on. The oscillation grows until it reaches a steady state at about 380 ms. The starting time of the oscillator with a 300 μm beam resonator is about 280 ms. The growth of the oscillation continues until 510 ms. These experimental results demonstrate that the starting time of the oscillator with the 400 μm beam resonator is a little faster than that of the oscillator with the 300 μm beam resonator.

The time required to reach a steady-state oscillation level is a function of the excess gain above unity and the input to output delay in the circuit. The delay primarily comes from the beam resonator. Reference 18 derives an expression for the delay t_d as a function of the loaded quality factor Q_l and the oscillation frequency ω_o:

$$t_d \equiv \left.\frac{d\varphi}{d\omega}\right|_{w=w_o} = \frac{2Q_l}{\omega_o}, \tag{22}$$

where φ is the phase and Q_l can be described in terms of the phase slope as a function of frequency. Equation (22) indicates that the starting time can be very long for an extremely high-Q device. The difference in the starting time between the oscillators with 400 μm and 300 μm beam resonators comes mainly from the loop gain because the loop gain at 0° of the oscillator with the 400 μm beam is greater than that of the oscillator with the 300 μm beam, whereas the measured Q_ls of the beam resonators are nearly the same as discussed in the open-loop measurements.

The waveform from the oscillator with the 400 μm beam resonator at steady-state oscillation is shown in Fig. 14(b). To operate the oscillator with a sinusoidal waveform the polarization voltage V_p was decreased to –0.15 V. As seen in Fig. 14(b), the oscillation frequency is about 280.9 kHz and the waveform is sinusoidal. The oscillation amplitude is about 150 mV.

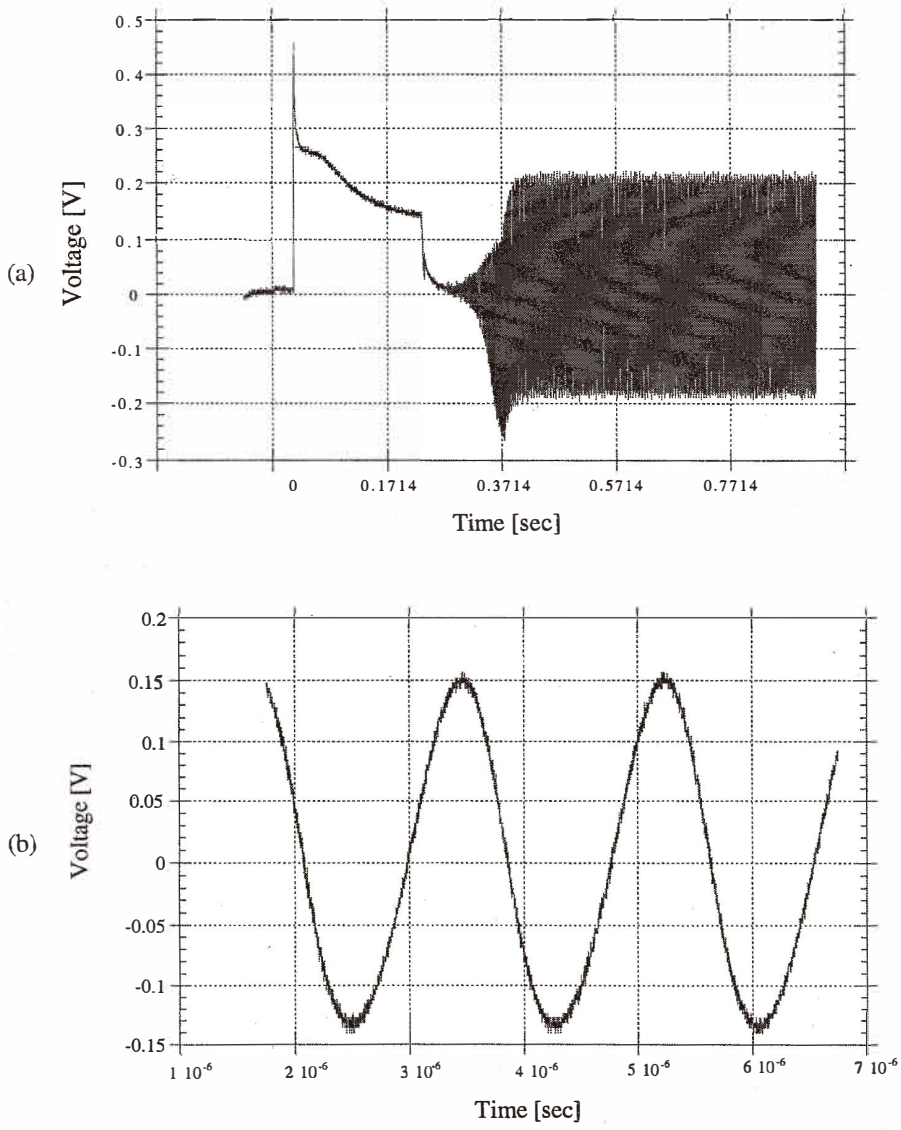

Fig. 14. Closed-loop measurements for a 400 μm simple beam resonator: (a) The evolution of the oscillations after turn-on. (b) Oscillogram showing the oscillation waveform for the oscillator with a 400 μm simple beam resonator at a steady state with the measured oscillation frequency f_o of 280.9 kHz.

3.3 *Amplitude stabilization of the oscillations*

A sinusoidal oscillator in which the loop gain is exactly unity is an idealization which is not realizable in practice. The loop gain becomes either less than or greater than unity in a very short time because the characteristics of circuit components and, more importantly, transistors change with age, temperature, voltage or other parameters. In every practical oscillator, the loop gain is slightly larger than unity and the amplitude of the oscillations is limited by some nonlinearity. Nonlinear oscillations produce large power dissipation in both the beam resonator and the amplifier circuit which results in component temperature increases. These cause changes in the oscillation frequency and the loaded Q. Two different methods for stabilizing the amplitude of the oscillations have been performed. A better design of the oscillator with the loop gain control scheme is shown in the following section.

3.3.1 *Amplitude stabilization with a small excess loop gain*

Experiments have been performed to operate the oscillator in the sinusoidal region with a small excess loop gain. This operation can be obtained by adjusting the loop gain with the polarization voltage V_p applied to the beam. Figure 15 shows the results. For the oscillator with the 400 μm beam resonator, sinusoidal oscillations are obtained at a low polarization voltage less than 0.5 V. The nonlinearity starts to occur when $V_p = -0.5$ V, as shown in Fig. 15. A very nonlinear waveform can be seen at $V_p = -2$ V. The waveform is limited due to saturation of the NMOS transistor. Table 2 summarizes the measured oscillation frequency of the closed-loop circuit as a function of the polarization voltage V_p. As shown in Table 2, the oscillation frequency decreases as the polarization voltage V_p increases. These experimental results support eq. (12), which theoretically describes DC polarization voltage effects on the resonant frequency of the microbeam resonators. The operation of the oscillator with a small polarization voltage involves low power dissipation in the beam resonator. The Q of the beam decreases as the DC voltage increases.

In controlling the loop gain of the oscillator for sinusoidal oscillations, much care is required to ensure that the loop gain does not fall below unity with variations in environmental parameters such as temperature and other circuit changes, as mentioned previously. Therefore, controlling by adjusting the polarization voltage V_p is not a good method for implementing a sinusoidal oscillator. Modifications of the circuit in Fig. 16 are necessary to stabilize the oscillation amplitude in the sinusoidal region.

3.3.2 *Amplitude stabilization by an active automatic gain control loop*

Another method of stabilizing the oscillation amplitude is the development of an automatic gain control (AGC) loop in the oscillator circuit. In this scheme the gain of the amplifier must be large. This results in a fast starting time and can be controlled by an AGC loop. Figure 16 shows a beam controlled oscillator with an active AGC loop. The amplifier and the active AGC loop in the oscillator circuit of Fig. 16 consist of p-channel and n-channel MOSFETs. A similar concept was proposed by Vittoz and Fallath[19] using weak inversion operation of MOSFETs for a quartz crystal oscillator. The concept of the loop gain control in the circuit of Fig. 16 is as follows:

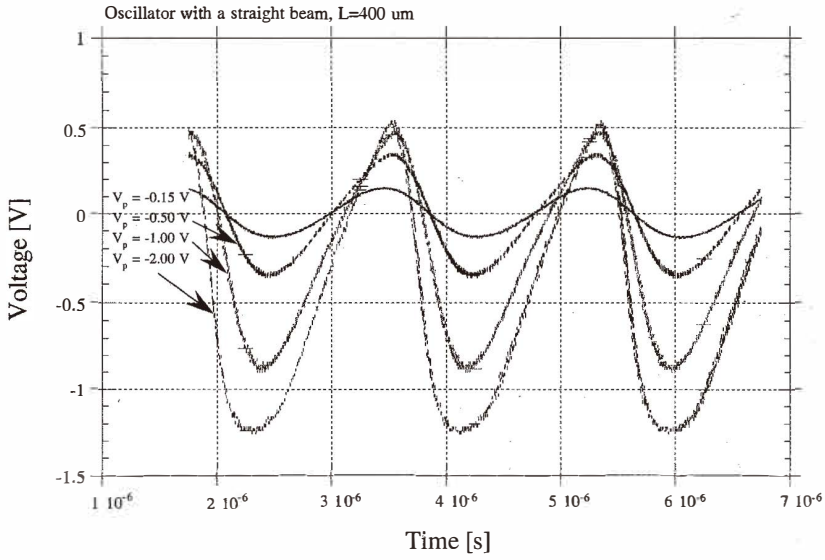

Fig. 15. Oscillogram showing the oscillation waveforms of the oscillator with a 400 μm beam resonator as a function of V_p. Nonlinearity starts to occur when $V_p = -0.5$ V.

Table 2
The oscillation frequency as a function of V_p. The power of the NMOS amplifier: 5 V for a 400 μm simple beam and 7.5 V for a 300 μm simple beam.

Polarization voltage, V_p	400 μm simple beam	300 μm simple beam
– 0.15 V	280.898 kHz	---
– 0.25 V	---	403.226 kHz
– 0.50 V	280.584 kHz	403.267 kHz
– 1.00 V	279.330 kHz	403.064 kHz
– 2.00 V	275.962 kHz	402.070 kHz

The beam resonator, the capacitances C_1 and C_2, and the transistors N_1, N_2 and N_3 constitute an oscillator biased by the diode D_1 and the current sources P_1, P_2 and P_3. When the DC power V_{DD} is turned on, the loop gain in the oscillator circuit is higher than one and the oscillation grows. The output of the oscillator is filtered by diode D_2 and capacitance C_3. The filtered DC voltage drives the inverter made up of the transistors N_4 and P_4 , whose output limits and controls the output characteristics of the transistors P_1, P_2 and P_3 to keep a constant amplitude of oscillation. With suitable design of the amplifier, the rectifier, and the inverter, the oscillation amplitude can be maintained in the sinusoidal region.

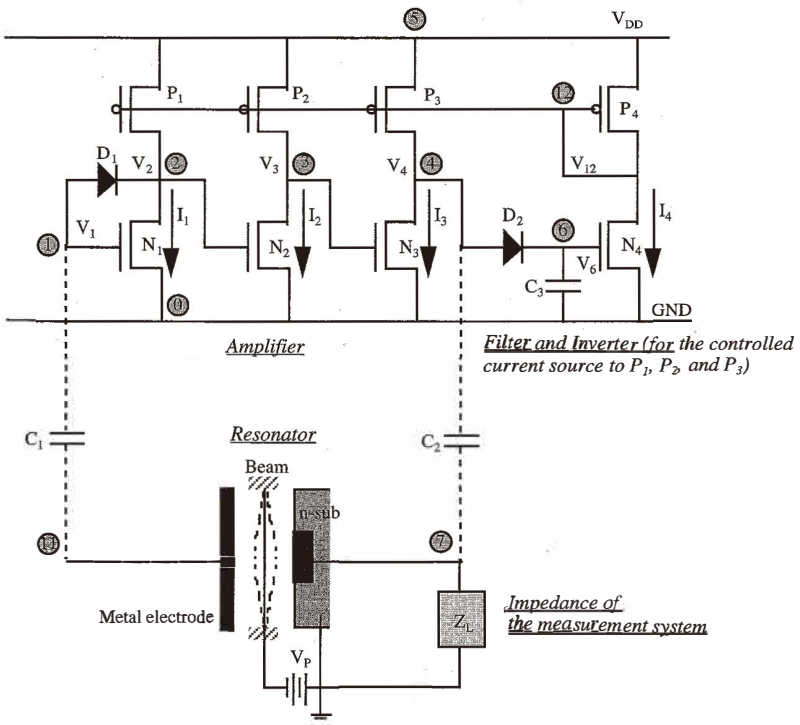

Fig. 16. An integrated beam controlled oscillator with an active AGC loop.

SPICE simulations with realistic circuit components were performed to design a beam controlled oscillator with an active AGC loop as shown in Fig. 16. Table 3 shows design parameters of the circuit for the SPICE simulations. The ratio of the channel width to the channel length for the p-channel and the n-channel MOSFETs are 20/5. A 5 V DC power supply is selected for the amplifier and the inverter. The electrical equivalent circuit of the beam resonator for the SPICE simulation is the same as that given in Fig. 7. The extracted electrical parameters from the beam resonator are determined by the experimental results of resonant frequency, quality factor and polarization voltage. Figure 17 shows the SPICE simulation results, which are the oscillation waveforms of the circuit at node 7 in Fig. 16 over various time periods. As shown in Fig. 17, the oscillation amplitude is kept at 120 mV and its waveform is maintained to be sinusoidal. The oscillation frequency is nearly the same as the resonant frequency of the beam. Table 4 shows the DC operating voltages and currents of the circuit at each node in Fig. 16. Using the data in Table 4, the static power dissipation of the circuit can be estimated and is calculated as about 2.23 mW.

An experiment using the beam controlled oscillator with an active AGC loop is performed using the available integrated circuits. The schematic diagram of the oscillator

Table 3
Design parameters of the circuit in Fig. 16 for the SPICE simulations.

NMOS (N_1, N_2, N_3, N_4)	
Threshold voltage	V_{tn} = 1.0 V
Oxide thickness	t_{ox} = 0.1 μm
Transconductance	$\mu_n C_{ox}$= 20 μ A/V^2
Body-effect coefficient	γ= 0.37 V$^{1/2}$
Lateral diffusion	L_D=1.0 μm
Gate-source overlap capacitance per meter channel width	C_{GSO}=345 pF/m
Gate-drain overlap capacitance per meter channel width	C_{GDO}=345 pF/m
Zero-bias junction sidewall capacitance per meter of junction perimeter	C_{SJW}=220 pF/m
Zero-bias junction sidewall capacitance per square meter of junction area	C_J=70 pF/m^2
Channel width/length	W/L=20/5 μm
PMOS (P_1, P_2, P_3, P_4)	
Threshold voltage	V_{tp}= – 1.0 V
Oxide thickness	t_{ox} = 0.1 μm,
Transconductance	$\mu_p C_{ox}$ =10 μA/V^2
Body-effect coefficient	γ= 0.37 V$^{1/2}$
Lateral diffusion	L_D=1.0 μm
Gate-source overlap capacitance per meter channel width	C_{GSO}=345 pF/m
Gate-drain overlap capacitance per meter channel width	C_{GDO}=345 pF/m
Zero-bias junction sidewall capacitance per meter of junction perimeter	C_{SJW}=220 pF/m
Zero-bias junction bottom capacitance per square meter of junction area	C_{JO}=70 pF/m^2
Channel width/length	W/L=20/5 μm
Diode (D_1, D_2)	
Junction saturation current	I_S = 0.1 pA
Junction ohmic resistance	R_S = 16 Ω
Zero-bias depletion capacitance	C_{JO} = 2 pF
Transit time	T_t=12 ns
Capacitance C_1, C_2, and C_3	
	C_1=C_2=10 nF
	C_3 =0.5 μF
Beam resonator (when V_p= 0.2 V and Q =10,000)	
Equivalent inductance	L_{eq}=1454.54062 H
Sensing capacitance	C_{so} = 233.3 fF
Equivalent inductance	R_{eq}= 365566 Ω
Driving capacitance	C_{do} = 70 fF
Equivalent capacitance	C_{eq} = 0.22212 fF
Other parasitics in the beam resonator:	
	R_{p1} = 100 MΩ
	R_{p2} = 100 GΩ
	C_{p1} = C_{p2} =1.0 pF
	C_{p3} = 0.5 fF

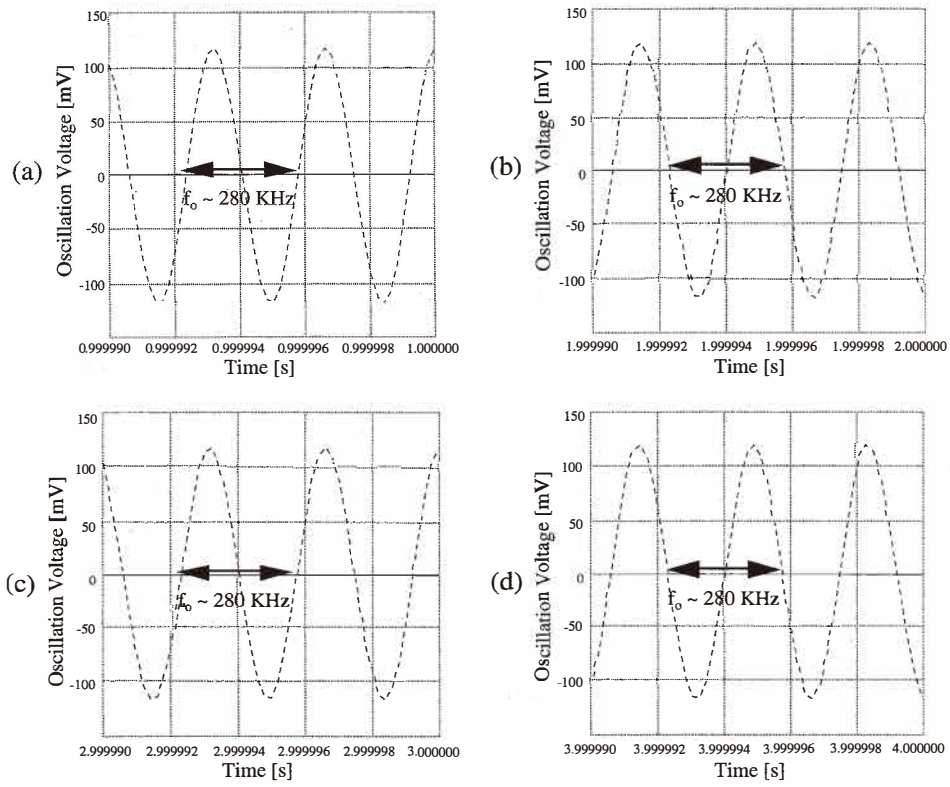

Fig. 17. SPICE simulation results. The oscillation waveforms of the circuit at node 7 in Fig. 16 over various time periods. The oscillation amplitude is kept at 120 mV and its waveform is maintained to be sinusoidal as time increases. The value of f_o is the oscillation frequency, which is almost the same as the resonant frequency, f_R of 280 kHz.

Table 4
DC operating voltages and currents of the circuit at each nodes in Fig. 16.

DC voltages at each node	DC currents at each node
$V_1 = 2.67004$ V	$I_1 = 111.560\ \mu$A
$V_2 = 2.67004$ V	$I_2 = 111.560\ \mu$A
$V_3 = 2.66800$ V	$I_3 = 111.290\ \mu$A
$V_4 = 2.75000$ V	$I_4 = 111.620\ \mu$A
$V_6 = 2.67050$ V	
V_{12}=1.63790 V	
$V_{DD} = 5.0$ V	$I_{total} = \sum_{n=1}^{4} I_n = 446.030\ \mu$A

circuit is shown in Fig. 18. In this circuit, the amplifier stage is modified. The amplifier stage consists of a two-stage CMOS amplifier and a one-stage NMOS amplifier. The concept of the loop gain control in Fig. 18 is the same as that in Fig. 16. To evaluate the performance of the active AGC loop, the DC polarization voltage applied to the micro-beam is varied. The measurement results are shown in Fig. 19. In this figure, the oscillation frequency decreases as the DC polarization voltage increases, but the oscillation amplitude stays at 340 mV peak-to-peak regardless of the DC polarization voltage changes.

4. Conclusion

The vacuum-encapsulated polysilicon beam resonators are transducers which can measure parameters such as pressure, temperature force, and acceleration. These devices produce changes in resonant frequencies when they are subjected to variation in the above

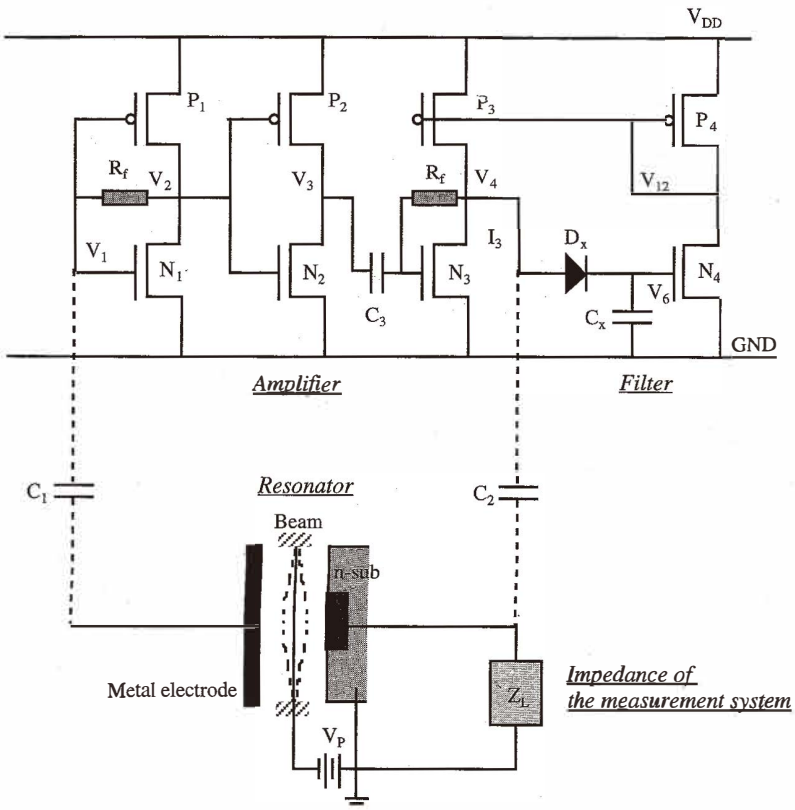

Fig. 18. Circuit diagram of a beam controlled oscillator with an AGC loop for experiments.

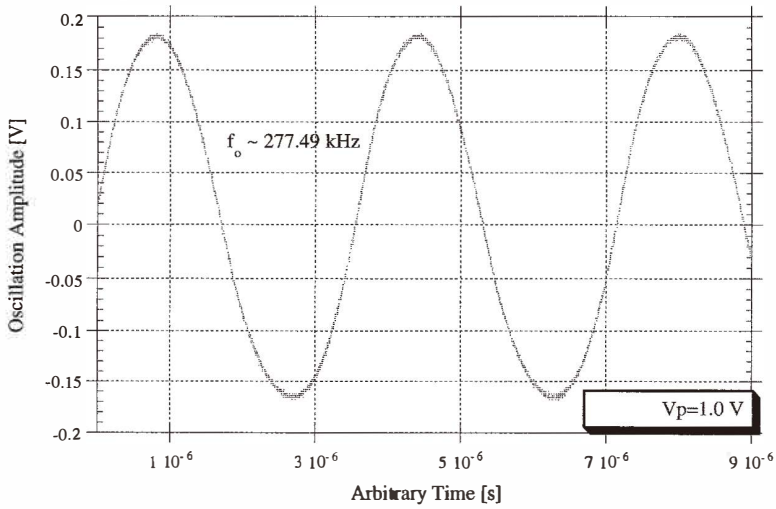

(a) V_p = 1.0 V, f_0 – 277.49 kHz

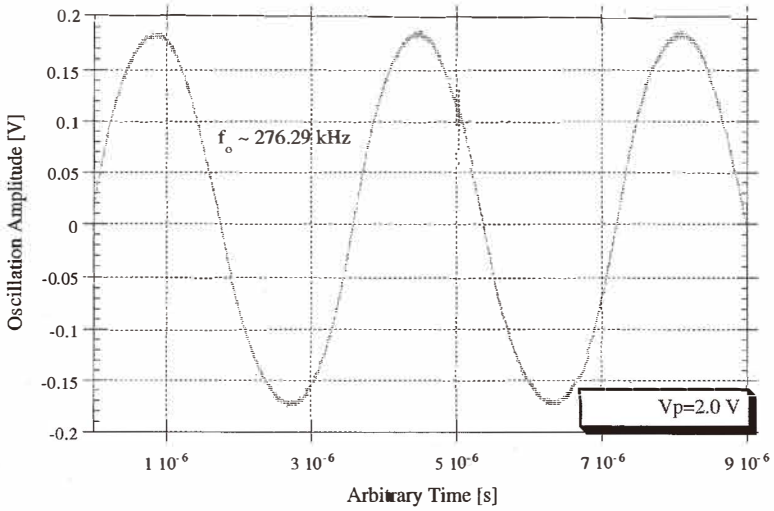

(b) V_p = 2.0 V, f_0 – 276.29 kHz

Fig. 19. Measured oscillograms of the beam controlled oscillator with an active AGC loop by changing the DC polarization voltages applied to the microbeam.

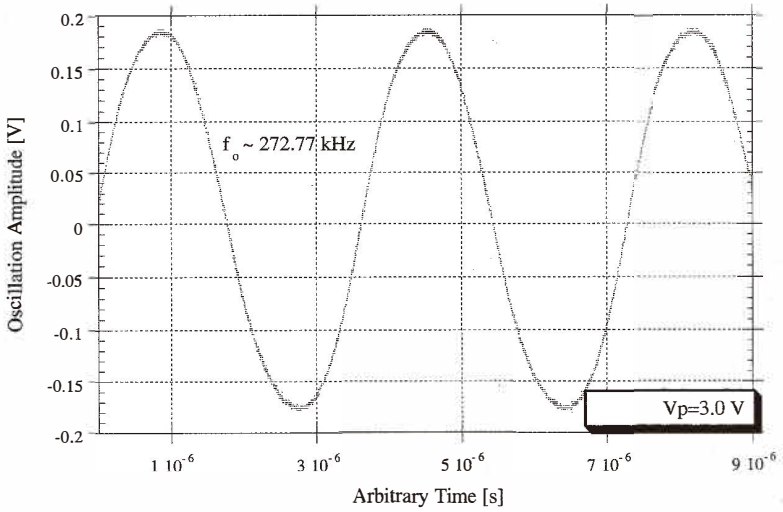

(c) V_p = 3.0 V, f_o ~ 272.77 kHz.

Fig. 19. Measured oscillograms of the beam controlled oscillator with an active AGC loop by changing the DC polarization voltages applied to the microbeam.

parameters.[1–6] Accurate frequency measurements require the implementation of an oscillator circuit with the microbeam resonator and microelectronics.

The principle advantages of the self-excited oscillator using a microbeam resonator are frequency outputs with good measurement stability and low power dissipation. Using polysilicon micromachining technology to fabricate the microbeams, it may also be possible to implement the oscillator via the cofabrication of microbeam resonators and microelectronics on a single chip.

A lumped circuit experiment with an oscillator using a microbeam and a MOS amplifier was performed on the basis of theory, mathematical calculation and SPICE simulations. The design of the microbeam resonators was optimized to minimize parasitics which affect the gain-phase response of the microbeams. Two-port beam resonators which have separate driving and sensing ports were selected for the beam controlled oscillator circuit. Oscillator circuits using two different microbeams with resonant frequencies at 280 kHz and 400 kHz exhibited oscillation behavior controlled by the beam resonant frequencies. A DC polarization voltage is required for the beam controlled oscillator with electrostatically driven microbeams, as opposed to quartz crystal and SAW oscillators in which the DC biases are not necessary.[19] An increase in the DC bias can easily cause mechanical instability of the microbeam. Increases in the DC polarization voltage applied to the microbeam result in decreases in resonant frequency and Q of the microbeam resonators. The drop in Q due to the DC polarization voltage is significant.

Therefore, an oscillator using a microbeam resonator must be designed to operate with low DC polarization voltages. Experiments indicate sinusoidal oscillation waveforms can be obtained by controlling the DC polarization voltages applied to the microbeams. This results in low power dissipation within the microbeam resonators. The oscillator also requires an AGC loop for long-term amplitude stabilization of the oscillations in the sinusoidal region. Extraction of the design parameters of an integrated sinusoidal oscillator with an active AGC loop has been performed for p-channel and n-channel MOSFETs. The SPICE simulation results indicate that the oscillation waveform of this circuit is controlled in the sinusoidal region without any amplitude change after the oscillation reaches a steady state. Experiments with an active AGC loop were performed and the results prove that this concept holds.

Acknowledgment

The authors thank Dr. J. D. Zook at the Honeywell Technology Center for valuable discussions and the staff of the Wisconsin Center for Applied Microelectronics for technical assistance. The authors acknowledge the Foxboro Company for funding part of this program.

References

1 J. D. Zook, D. W. Burns, H. Guckel, J. J. Sniegowski, R. L. Engelstad and Z. Feng: Sensors and Actuators A **35** (1992) 51.
2 J. W. Kang: Ph.D. Thesis, University of Wisconsin-Madison, USA, May (1996).
3 H. Guckel: Sensors and Materials **4** (1993) 251.
4 H. Guckel, M. Nesnidal, J. D. Zook and D. W. Burns: Transducers '93, Proc. of 7th Intl. Conf. on Solid-State Sensors and Actuators, Yokohama, Japan (1993) p. 686.
5 H. Guckel: Phil. Trans. R. Soc. Lond. A **353** (1995) 355.
6 H. Guckel, J. J. Sniegowski, T. R. Chritenson and F. R. Rassi: Sensors and Actuators A **21**– **23** (1990) 346.
7 B. W. Burns: Ph.D. Thesis, University of Wisconsin-Madison, USA, Aug. (1988).
8 J. J. Sniegowski: Ph.D. Thesis, University of Wisconsin-Madison, USA, Dec. (1991).
9 H. Guckel: Sensors and Actuators A **28** (1991) 133.
10 J. D. Zook, D. W. Burns, J. N. Schoess and H. Guckel: SPIE Proc., Vol. 2383A, Conf. Miniaturized Systems with Micro-optics and Micromechanics, Photonics 1995, San Jose, CA, USA, February (1995).
11 J. D. Zook , D. W. Burns, W. R. Herb, H. Guckel, J. W. Kang and Y. Ahn: Sensors and Actuators A **52** (1996) 92.
12 Test and Measurement Catalogs, John Fluke Mfg. Co., Inc. and Phillips Test and Measurement Dept. (1989).
13 Test and Measurement Catalog, Hewlett-Packard Co. (1989).
14 Test and Measurement Catalog, Tektronix Inc. (1989).
15 Y. Ahn: Ph.D. Thesis, University of Wisconsin-Madison, USA (1999).
16 J. Zook, W. R. Herb, Y. Ahn and H. Guckel: J. Vac. Sci. Technol. A **17** Jul/Aug (1999) 2286.
17 HSPICE, Meta-Software and PSpice, MicroSim.
18 R. W. Rhea: Oscillator Design & Computer Simulation, 2nd Ed., McGraw-Hill (1997).
19 E. Vittoz and J. Fellath: IEEE Journal of Solid-State Circuits Vol. SC-**12** No.3 June (1977) 224.